

Global Flow Regime Identification of Adiabatic Upward Two-phase Flow in a Vertical Rod Bundle Geometry

Sidharth Paranjape*, Yong Liang, Damian Stefanczyk,

Takashi Hibiki and Mamoru Ishii

School of Nuclear Engineering, Purdue University

400 Central Dr., West Lafayette, IN 47907-2017, USA

* Corresponding author

Tel: +1-765-494-5759, Fax: +1-765-494-9570, Email: paranjap@purdue.edu

ABSTRACT

Flow regime maps were obtained for an adiabatic air-water two phase flow through a flow channel with 8×8 rod bundle, which simulated a typical rod bundle in a boiling water reactor. Impedance void meters were used to measure the area averaged void fraction at various axial locations in the flow channel. The Cumulative Probability Distribution Functions (CPDF) of the signals from the impedance meters were fed to a self organizing neural network to identify the flow regimes. The flow regimes were identified at seven axial locations in the channel in order to understand the development of the flow regimes in axial direction. The experimental flow regime transition boundaries agreed well with the theoretical ones obtained using Mishima and Ishii (1984) model. In addition, the two impedance void meters located across a spacer grid, which were used to study the change in the flow regime across the spacer grid.

1. INTRODUCTION

Identification of flow regimes is the first logical step in the analysis of a two phase flow system, since it signifies the geometrical structure of the two-phases. The analysis of two phase flow through a rod bundle is of particular interest to Boiling Water Reactor (BWR) safety research. In the current state, most of the safety analysis codes utilize the flow regime maps developed for two-phase flow through circular channels. Hence, it is necessary to obtain flow regime map for two phase flow through a rod bundle geometry. Though many researches have been carried out for understanding the flow regimes through a rod bundle [1-4], the knowledge of flow regime boundaries is still rudimentary. This is attributed to the identification method used in the previous researches. All of the previous researches in rod bundle two-phase flow were based on flow visualization, which introduced subjectivity in the identification. In addition, the definitions of the flow regimes were not clear as visualization through the rod bundles imposed significant problems. However, it is worthwhile to note the flow regime study carried out by Mizutani et al. [4]. They used transparent rods having similar refractive index as water, which facilitated flow visualization. They also performed detailed flow visualization in sub-channels.

Though the geometrical structure of a two phase flow can best be identified by flow visualization, most of the modern techniques use analysis of the time series signals obtained from various instruments such as differential pressure cells, impedance void meters etc. in order to eliminate the subjectivity [5-7]. The flow regime at a given cross section of a two phase flow channel can be identified by analyzing the variation of void fraction at that location. In the current study, impedance void meters are used to measure the area averaged void fraction in a flow channel with 8×8 rod bundle simulating a typical rod bundle in a BWR. The experiments are carried out in air-water two-phase flow under adiabatic conditions. The Cumulative

Probability Distribution Functions (CPDF) of the signals from the impedance meters is fed to a self organizing neural network to identify the flow regimes. Since the information is averaged over the cross section of the channel, it is referred to as global flow regime. The flow regimes are identified at four axial locations in the channel, which highlights the development of the flow regimes in axial direction. In addition, the two impedance void meters located across a spacer grid, which are used to study the change in the flow regime across the spacer grid.

2. EXPERIMENT

2.1 Experimental Facility and Instrumentation

A general outline of the test facility that was used for the measurement of two-phase flow parameters in the rod bundle geometry is shown in Figure.1. The test section consisted of a 3 m long vertical flow channel with square cross section having sides of length 140 mm. It housed an 8×8 array of 64 acrylic rods each having a diameter of 12.7 mm arranged at a pitch distance of 16.7mm. The distance between the center of the peripheral rod and side wall is 11.6 mm. Table 1 summarizes the geometric parameters of interest. The acrylic rods were held in place by six spacer grids located at $z/D_H = 31, 61, 91, 121, 151$ and 180. Here, D_H is the hydraulic diameter of a typical subchannel and z is the axial distance from the inlet of the test section. The hydraulic diameter of a typical subchannel is 14.8 mm. The walls of the test section were made out of acrylic, which allowed flow visualization using a high speed camera. Air-water mixture was injected into the test section using an air-water mixture injection unit which consisted of an 8×8 array of spargers located beneath the acrylic rods, as shown in Figure.2. Each sparger was surrounded by a stainless steel tube. The water flowing through the annular space between this tube and the sparger was used to shear-off the bubbles coming out of the

porous sparger. The air-water mixture injection unit was designed to inject finely dispersed bubbly flow into the bottom of the test section with bubbles of approximately uniform diameter of 1 mm.

The water flow was supplied by a 75 hp centrifugal pump. The volumetric liquid flow rate was measured by an electromagnetic flow-meter having an accuracy of ± 1 %. The air flow was measured with Venturi flow meters. Three flow meters having different measurement range were connected in parallel so as to allow the measurement of air flow rate up to 15 m/s in the test section. The pressure difference measured across the Venturi flow meters was then converted to flow rate through a manufacturer supplied calibration. The accuracy of the Venturi meters is ± 0.5 %. In addition to the flow measuring instruments, a thermocouple was used to measure the inlet water temperature and a thermometer installed in the inlet air pipe was used to measure inlet air temperature with an accuracy of 0.1 degree Celsius.

The test section was equipped with seven impedance meters for the measurement of area averaged void fraction in the test section at various axial locations. An impedance void meter is a non-intrusive conductance type probe that utilizes the difference in electrical conductivity between the air and water. The impedance meter consisted of two parallel plate type electrodes located on the opposite walls of the test section, spanning the length of the sides. The electrodes had width of 9.5 mm in axial direction. An alternating current was supplied to the electrodes and the electrodes were connected to the electronic circuit, which was specially designed so that the output voltage of the circuit was proportional to the measured impedance between the electrodes. In addition, pressure taps were provided at each axial location in the test section along with the impedance meters. A differential pressure cell having an accuracy of ± 0.5 % was used to measure the differential pressure along the flow channel. A pressure

gauge was installed at the first measurement port of the test section. The impedance meters and the pressure taps were located at the axial distances of $z/D_H = 7, 86, 94, 116, 124, 137$ and 200 .

The impedance meters were calibrated against the void measurements using differential pressure transducers under stagnant liquid phase condition. Under this condition, accelerational and frictional pressure drops were negligible compared to the gravitational pressure drop. Void fraction could be obtained by equating the measured pressure drop to the two-phase gravitational pressure drop. It was found that the relation between the void fraction and the normalized impedance was linear. The measurement accuracy of the impedance void meter was estimated to be within $\pm 10\%$. The details of experimental facility and instrumentation are found in [8].

2.2 Experimental Methodology

The experiments were carried out at various inlet volumetric fluxes of air and water. The outlet of the test section was open to a tank at atmospheric pressure. Thus the outlet boundary condition was at a fixed pressure. The experimental conditions were identified by the inlet area averaged flow velocities. The inlet superficial gas velocity, $\langle j_g \rangle$, ranged from 0.02 m/s to 10 m/s, while the superficial liquid velocity, $\langle j_l \rangle$, ranged from 0.02 m/s to 1.5 m/s. Figure 3 shows the measured flow conditions. At each flow condition, the data from all the instruments were scanned at the rate of 1000 Hz for total time period of 60 seconds. The data acquisition frequency gave sufficient time resolution for current range of the flow rates, while the time duration was sufficient to yield statistically stable results.

Over the years many statistical parameters have been used to objectively identify and characterize the two-phase flow regimes in pipe. For example Probability Density Function (PDF) of the void fraction signal or pressure drop fluctuation signal has been widely used for the

flow regime identification [9]. Researchers have also used the statistical parameters such as standard deviation and Cumulative PDF (CPDF) of the signal in order to discriminate the various flow regimes. A significant advancement in the objective flow regime identification was achieved by Mi et al. [5, 10]. Using the statistical parameters from the PDF of impedance probes and Kohonen self-organizing neural networks they were able to identify the flow regimes for a vertical upward two-phase flow with more objectively. The main drawback of this approach laid in the long duration of the observation needed to obtain reliable statistical parameters of the void fraction signal [6]. Afterward it was found that the use of an integral parameter such as CPDF of the signal instead of PDF was more stable [7]. In addition, it has smaller input data requirement that makes it useful for the fast identification process.

3. RESULTS AND DISCUSSION

3.1 Flow Regime Visualization Using High-Speed Camera

As a first step towards the analysis, flow visualization study was carried out to understand the overall flow structure in the 8×8 rod bundle geometry. The transparent acrylic walls of the test section allowed visualization of the whole flow. A high speed camera (up to 5000 frames per second) was used to visualize the flow structure. Figure 4 shows the snap-shots from the videos obtained for various flow conditions at $z/D_H = 140$. In a broad sense, following flow regimes were observed in the current experimental conditions.

1. Bubbly flow: This flow regime consisted of dispersed spherical and distorted-spherical bubbles throughout the test section. The bubble sizes ranged from 2 mm to 10 mm approximately. The bubbles were present in the sub-channels as well as in the gap

between the rods. Though most of the bubbles moved in the flow direction in a subchannel, they often migrated to neighboring ones. It should be noted that the elongated bubbles in Figure 4(a) are indeed spherical bubbles crossing the rod gaps. They appeared elongated because of optical distortion due to difference in the refractive indices of acrylic and water.

2. Cap-Bubbly flow: As the bubble size grew, cap shaped bubbles were observed along with the spherical ones, which spanned a typical subchannel and often spanned two subchannels. Migration of bubbles through the rod gaps was also observed in this case. In this flow regime, the cap bubble motions were found to be relatively steady.
3. Cap-Turbulent flow: As the velocity of gas flow was increased for a given liquid flow rate, cap bubbles grew in size, often spanning more than two subchannels. The motion of the cap bubbles was observed to be turbulent.
4. Churn-Turbulent flow: Large bubbles spanning five to six subchannels were observed in this flow condition with highly agitated motion. The bubbles often moved in a zigzag manner through the whole test section.

It should be noted here that no stable slugs were observed. Hence slug flow regime was not recognized in the current conditions. No Taylor bubble spanning the whole cross section, as described by Venkateswararao et al. [3] was observed in the current geometry. This is expected, since the length of the side of the bundle test section (140 mm) is larger than the maximum cap bubble size (100 mm) for air-water flow under room temperature and atmospheric pressure [11]. Furthermore, annular flow was not observed in the current conditions.

3.2 Drift-Flux Plot for Two-Phase Flow in 8×8 Rod Bundle Geometry

In the previous section the flow regimes were subjectively identified by visualization. This warrants the need for objective flow regime identification using impedance void meter signals along with neural network methodology. As described in the previous section, impedance void meter signals were used along with neural network methodology to identify the flow regimes. The neural network was programmed to classify the data into four categories, which were physical interpreted as stated in the previous section. In the next section, the results are compared with the flow regime transition criteria obtained by Mishima and Ishii [12], which is well-established to predict the flow regime transition boundaries for upward two-phase flow in a vertical round pipe. The computation of the flow regime transition boundaries by Mishima-Ishii's model requires the information of the distribution parameter, C_0 , and drift velocity, $\langle\langle v_{gj} \rangle\rangle$, in the drift-flux model for 8×8 rod bundle test section. The one-dimensional drift-flux model is expressed as [13]:

$$\langle\langle v_g \rangle\rangle = \frac{\langle j_g \rangle}{\langle \alpha \rangle} = C_0 \langle j \rangle + \langle\langle v_{gj} \rangle\rangle, \quad (1)$$

Where $\langle\langle v_g \rangle\rangle$, $\langle \alpha \rangle$ and $\langle j \rangle$ are, respectively, the void fraction weighted mean gas velocity, area-averaged void fraction and mixture volumetric flux. In what follows, the distribution parameter and drift velocity are obtained using newly obtained experimental data.

Since the superficial gas and liquid velocity are measured by the flow meters and void fraction by impedance void meters, the plot of $\langle\langle v_g \rangle\rangle$ vs. $\langle j \rangle$ can be used to obtain the drift-flux parameters. Figure 5 suggests that these parameters are $C_0=1.05$ and $\langle\langle v_{gj} \rangle\rangle=0.123$ m/s. These two drift-flux model parameters are in good agreement with those found by Yun et al. [14] for 3×3 rod bundle test section and were utilized to obtain the transition boundaries by Mishima

and Ishii. The hydraulic diameter of the whole test section (14.8 mm) was used for obtaining the transition boundaries.

3.3 Objective Flow Regime Identification Using Neural Network

Figure 6 shows the experimental flow regime map at $z/D_H=200$ obtained using the impedance void meter along with the neural network methodology. The symbols show the experimental flow conditions, while the thicker and thinner lines indicates the flow regime transition boundaries determined by neural network and Mishima-Ishii's transition criteria model, respectively. It is interesting to observe that the transition from bubbly to cap-bubbly flow agrees well with the theoretical transition from bubbly to slug flow, $\langle\alpha\rangle=0.3$. The experimental cap-bubbly and cap-turbulent regime corresponds to the slug flow regime in a small round pipe. It is noted that the transition from cap-turbulent to churn-turbulent flow agrees well with the theoretical transition from slug to churn flow in the current range of superficial gas and liquid flow rates.

Since the global flow regime transition may be expected to depend on the overall size of the test section, it is worthwhile to compare the experimental observations with flow regimes obtained in flow channels of similar size. Smith et al. studied flow regime transitions in circular tubes of 102 mm and 152 mm internal diameters [15]. The width of the test section square wall (140 mm) lies between those of the two flow channels. Impedance void meter signals with neural network methodology were used to classify the data into three flow regimes, namely bubbly, cap-bubbly and churn-turbulent. Slug flow was not observed, since the diameters of the tubes were larger than the maximum cap bubble size, i.e., 100 mm.

Figure 3 shows the comparison of current experimental data with the experimental transition boundaries obtained for 102 mm and 152 mm ID test sections. In the figure, thicker solid and dotted lines, respectively, indicate the flow regime transition boundaries between bubbly and cap bubbly flows for 102 mm ID test section, whereas thicker broken and chain lines, respectively, indicate the flow regime transition boundaries between bubbly and cap bubbly flows for 152 mm ID test section.

The transition boundary from bubbly to cap bubbly flow for 102 mm ID test section is close to the cap-bubbly to cap turbulent flow regime boundary identified in the rod bundle geometry, while the cap-bubbly to churn-turbulent boundary is close to cap-turbulent and churn-turbulent transition of the current data. The transition line for bubbly to cap bubbly regime obtained for 152 mm ID test section is closer to the bubbly to cap bubbly transition obtained in the present case, since the width of square wall of the present test section is closer to 152 mm ID test section. In addition, it should be noted that Smith et al. did not classify the flow regimes into four categories in contrast to the present case [15].

Figure 3 also compares the experimental flow regime map with the Mishima-Ishii's transition criteria with $D_H=140$ mm instead of $D_H=14.8$ mm for the whole test section. In the figure, Mishima-Ishii's transition criteria are indicated by thinner lines. In this case, the transition from bubbly to cap-bubbly flow regime compares well with the theoretical transition criteria for bubbly to slug flow regime. This is expected, since the transition boundary is based on the formation of cap or slug bubbles at the void fraction of 0.3. However, the mechanism of the transition from slug to churn-turbulent flow is not applicable for the flow channels with a hydraulic diameter greater than maximum cap bubble size. Hence the transition from cap-turbulent to churn-turbulent does not agree with that obtained by theoretical transition criterion

for the flow channel with the hydraulic diameter of 140 mm. Currently, no theoretical transition criteria is available for cap-bubbly to churn-turbulent flow regimes observed in flow channels with diameters larger than the maximum cap bubble size.

The presence of multiple impedance probes at several axial locations in the flow channel made it feasible to study the development of the flow structure in the flow direction. It was observed that the flow regimes developed within a short flow channel length. Figure 7 shows the experimental flow regime map at the first measurement port, $z/D_H=7$, along with the Mishima-Ishii's transition criteria with $D_H=14.8$ mm. The comparison between Figures 6 and 7 clearly indicates that the experimental flow regime map agrees well as in a case of the map obtained at $z/D_H = 200$.

3.4 Effect of Space Grids on Flow Structure

The existence of spacer grids in the flow affects the flow structure significantly, though for a relatively short distance in the flow direction. As expected, the formation of the wake structure in the downstream direction of a spacer grid alters the distribution of bubble sizes in that region. Two impedance meters were located across a spacer grid positioned at the axial location of $z/D_H=121$. The experimental flow regime transition boundaries obtained from the signals of upstream ($z/D_H=116$) and downstream ($z/D_H=124$) impedance meters is shown in Figure.8. It can be observed that the impact of the spacer grid is different for different superficial liquid velocities. For low superficial liquid velocities, i.e. $\langle j_l \rangle < 0.25$ m/s, the flow regime transition boundaries shift towards higher superficial gas velocities. This suggests that presence of spacer grid promotes bubble breakup. The trend is reversed for superficial liquid velocities higher than 0.25 m/s, suggesting bubble coalescence.

From this observation it can be inferred that wake region downstream of the spacer grid is larger for higher superficial liquid velocities promoting agglomeration of bubbles in that region. The qualitative visual observation supports this inference. In order to study the extent of the impact of the spacer grid on flow structure, flow regime map was obtained from the impedance meter located further downstream of the spacer grid (at $z/D_H=137$). It is evident from Figure.9 that the flow structure develops within the distance of $16D_H$ ($=23.7$ cm) to its original state, since the flow regime map is very similar to the one obtained for the port located at $z/D_H=200$. Thus, though a spacer grid modifies the flow structure in its vicinity, it does not have significant impact on the overall axial development of the flow structure.

4. CONCLUSION

Air-water two-phase flow experiments were performed in an 8×8 rod bundle test section to obtain flow regime maps at various axial locations. The ranges of area averaged superficial gas and liquid velocities were $0.02 < \langle j_g \rangle < 10$ m/s and $0.02 < \langle j_f \rangle < 1.2$ m/s. Area averaged void fraction was measured using parallel plate type impedance void meters. The cumulative probability distribution functions of the signals from the impedance void meters were used along with a self organizing neural network to identify flow regimes. Four flow regimes were identified in the current geometry and the range of flow conditions, namely bubbly, cap-bubbly, cap-turbulent and churn-turbulent. The following significant conclusions were made from the current experimental study.

1. The distribution parameter and the void weighted drift velocity were found to be 1.05 and 0.12 m/s, respectively.

2. The experimental flow regime map agreed well with the flow regime transition boundaries given by Mishima and Ishii [12]. The cap-bubbly and cap-turbulent regimes corresponded to the slug regime defined by Mishima and Ishii [12].
3. It was found that the net hydraulic diameter of the test section (14.8 mm) should be used for theoretical predictions of transition boundaries rather than the square wall hydraulic diameter (140 mm).
4. The impact of spacer grids was significant on the flow regime map in the immediate downstream vicinity. However, the flow structure developed within a short distance ($z < 16D_H$) downstream of the spacer grid.

ACKNOWLEDGEMENT

This work was performed at Purdue University under the auspices of the U.S. Nuclear Regulatory Commission (NRC), Office of Nuclear Regulatory Research, through the Institute of Thermal-Hydraulics. The authors would like to express their sincere appreciation to NRC staffs for their continuous support on this program.

NOMENCLATURE

C_0 Distribution Parameter

D_H Hydraulic equivalent diameter [m]

j Total volumetric flux [m/s]

j_l Superficial liquid velocity [m/s]

j_g Superficial gas velocity [m/s]

v_g Gas velocity [m/s]

v_{gj} Drift velocity [m/s]

Greek Symbol

α Void fraction [-]

Symbols

$\langle \rangle$ Area averaged quantity

$\langle \langle \rangle \rangle$ Void fraction weighted mean quantity

REFERENCES

1. Bergles, A. E., Roos, J. P. and Bourne, J. G., 1968, "Investigation of boiling flow regimes and critical heat flux," NYO-3304-13, Dynatech Corporation, Cambridge, Massachusetts, USA.
2. Williams, C. L. and Peterson Jr., A. C., 1978, "Two phase flow patterns with high pressure water in a heated four-rod bundle," Nuclear Science and Engineering, 68, pp. 155-169.
3. Venkateswararao, P., Semiat, R. and Dukler A. E., 1982, "Flow pattern transition for gas-liquid flow in a vertical rod bundle," International Journal of Multiphase Flow, 8, pp. 509-524.
4. Mizutani, Y., Tomiyama, A., Hosokawa, S., Sou, A., Kudo, Y. and Mishima, K., 2007, "Two-phase flow patterns in a four by four rod bundle," Journal of Nuclear Science and Technology, 44, pp. 894-901.
5. Mi, Y., Ishii, M. and Tsoukalas, L. H., 1998, "Vertical two-phase flow identification using advanced instrumentation and neural networks," Nuclear Engineering and Design, 184, pp. 409-420.

6. Julia, J. E., Liu, Y., Paranjape, S. and Ishii, M., 2008, "Upward vertical two-phase flow local flow regime identification using neural network techniques," *Nuclear Engineering and Design*, 238, pp.156-169.
7. Lee, J. Y., Ishii, M. and Kim, N. S., 2008, "Instantaneous and objective flow regime identification method for the vertical upward and downward co-current two-phase flow," *International Journal of Heat and Mass Transfer*, 51(13-14), pp.3442-3459.
8. Paranjape, S., Stefanczyk, D., Liang, Y., Hibiki, T. and Ishii, M., 2008, "Global flow regime identification in a rod bundle geometry," *Proceedings of the 16th International Conference on Nuclear Engineering*, May 11-15, 2008, Orland, Florida, USA, ICONE16-48435.
9. Jones, O. C. and Zuber, N., 1975, "Interrelation between void fraction fluctuations and flow patterns in two-phase flow," *International Journal of Multiphase Flow*, 2, pp. 273-306.
10. Mi, Y., Ishii, M. and Tsoukalas, L. H., 2001, "Flow regime identification methodology with neural networks and two-phase flow models," *Nuclear Engineering and Design*, 204, pp. 87-100.
11. Kataoka I. and Ishii M., 1987, "Drift-flux model for large diameter pipe and new correlation for pool void fraction," *International Journal of Heat and Mass Transfer*, 30, pp. 1927-1939.
12. Mishima, K. and Ishii, M., 1984, "Flow regime transition criteria for upward two-phase flow in vertical tubes," *International Journal of Heat and Mass Transfer*, 27, pp. 723-737.
13. Zuber, N. and Findlay, J. A., 1965, "Average volumetric concentration in two-phase flow systems," *Journal of Heat Transfer*, 87, pp. 453-468.
14. Yun, B. J., Park, G. C., Julia, J. E. and Hibiki, T., 2008, "Flow structure of subcooled boiling water flow in a subchannel of 3×3 rod bundles," *Journal of Nuclear Science and Technology*, 45, pp. 1-21.

15. Smith, T., Ishii, M., Mi, Y. and Aldorwish, Y., 2001, “Flow regime identification using impedance meters and self-organizing neural networks for vertical pipe sizes: ½”, 2”, 4”, 6” ID,” Proceedings of the 4th International Conference on Multiphase Flow, May 27-June 1, 2001, New Orleans, Louisiana, USA, ICMF4-767.

Figure Captions

- Figure 1. Schematic diagram of the experimental test facility.
- Figure 2. Schematic diagram of air-water mixture injection.
- Figure 3. Comparison of experimental flow regime map at $z/D_H=200$ with experimental transition boundaries observed in 102 mm and 152 mm ID round pipe test sections [15].
- Figure 4. Flow visualization in various flow regimes at $z/D_H=140$.
- Figure 5. Drift-flux plot.
- Figure 6. Experimental flow regime map at $z/D_H=200$.
- Figure 7. Experimental flow regime map at $z/D_H=7$.
- Figure 8. Experimental flow regime maps across the spacer grid at $z/D_H=121$, with upstream port at $z/D_H=116$ and downstream port at $z/D_H=124$.
- Figure 9. Experimental flow regime map at $z/D_H=137$.

Table 1. Geometric parameters of test section.

	Area [mm ²]	Perimeter [m]	Hydraulic Diameter [m]
Total Cross Section	1.15×10^4	3.11×10^3	14.8
Inner Subchannel	152	40	15.3
Side Subchannel	130	37	14.1
Corner Subchannel	102	33	12.3

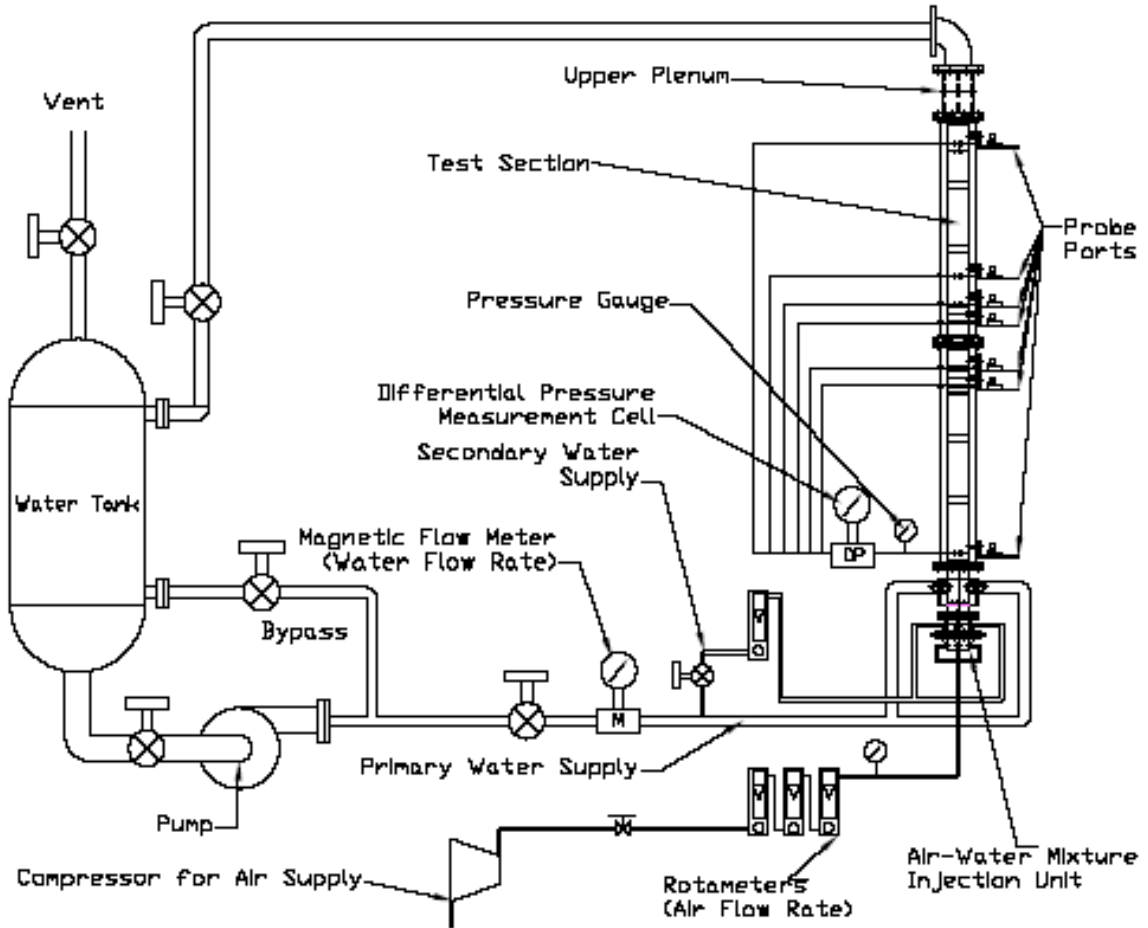


Figure 1. Schematic diagram of the experimental test facility.

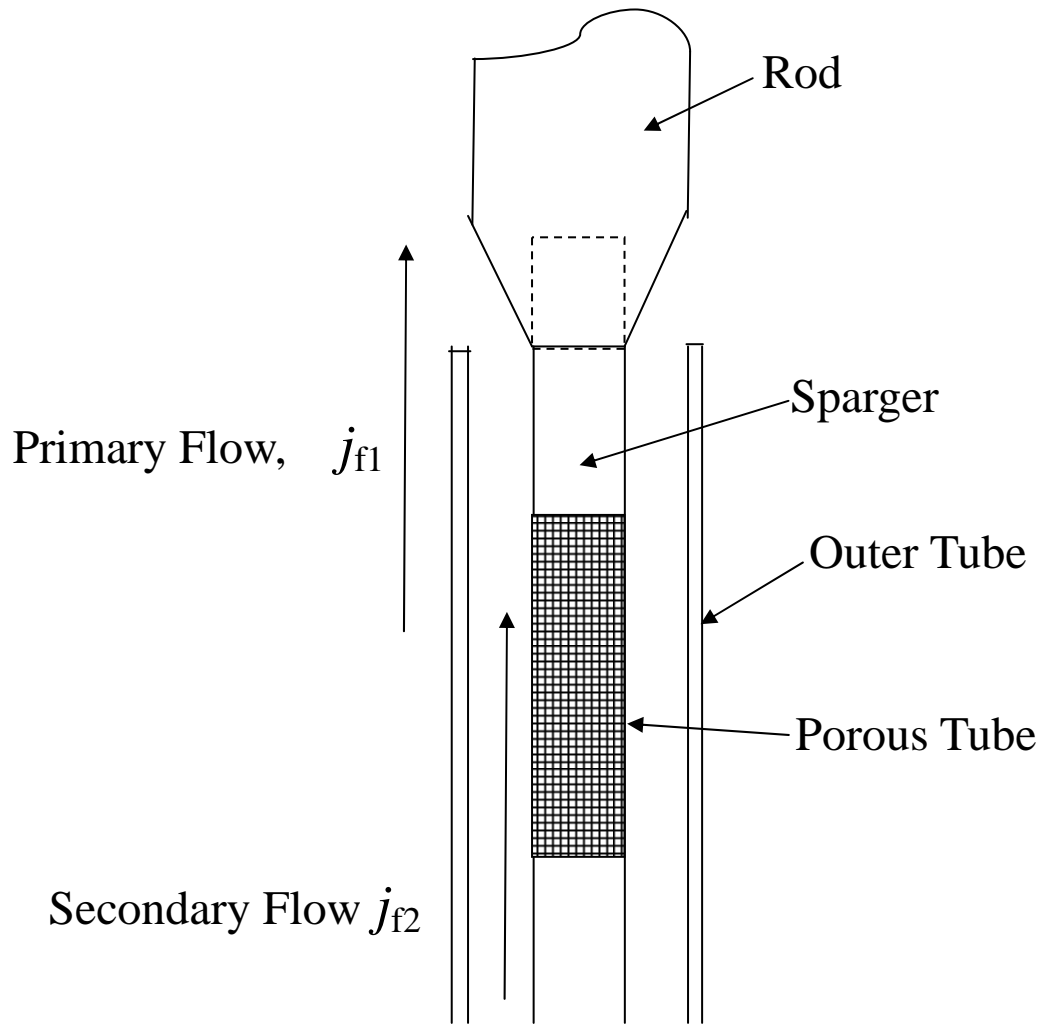


Figure 2. Schematic diagram of air-water mixture injection.

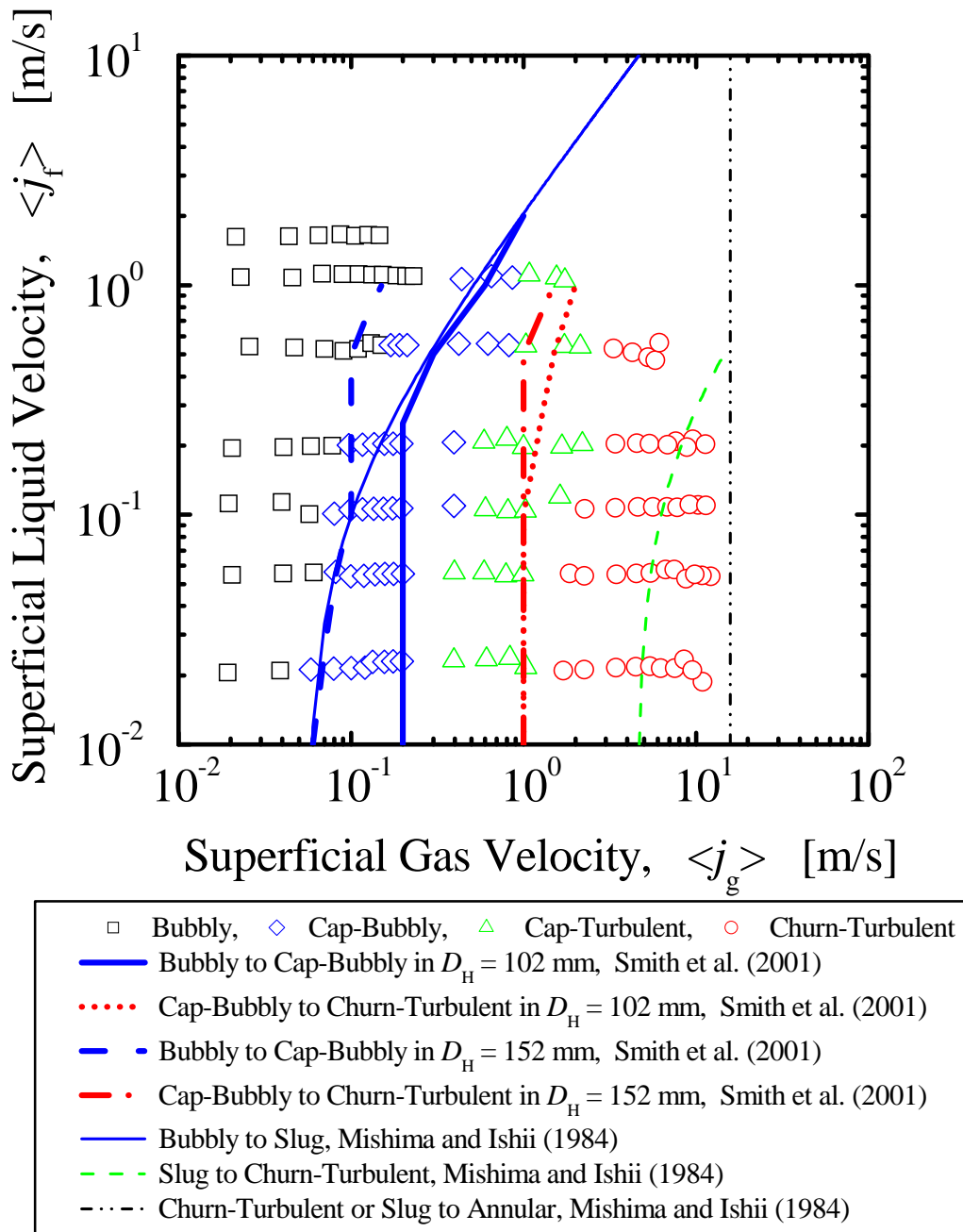
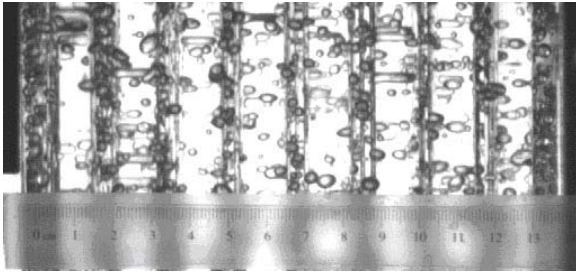
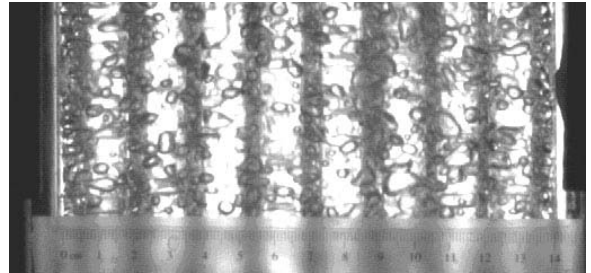


Figure 3. Comparison of experimental flow regime map at $z/D_H=200$ with experimental transition boundaries observed in 102 mm and 152 mm ID round pipe test sections [15].



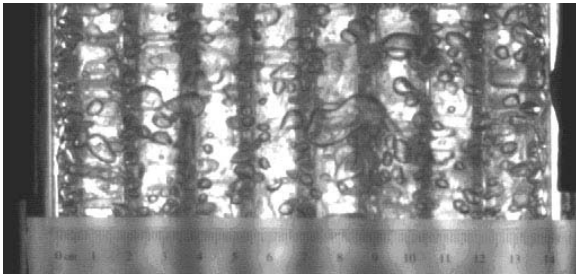
(a) Bubbly flow

$$\langle j_g \rangle = 0.02 \text{ m/s}, \langle j_f \rangle = 0.20 \text{ m/s}.$$



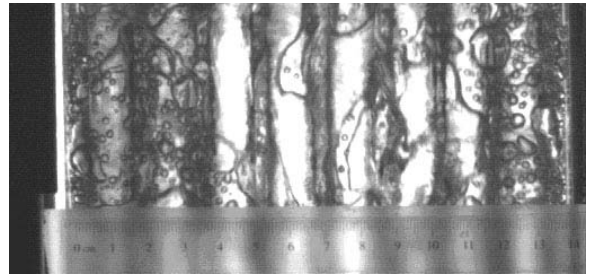
(b) Cap bubbly flow

$$\langle j_g \rangle = 0.14 \text{ m/s}, \langle j_f \rangle = 0.20 \text{ m/s}.$$



(c) Cap turbulent flow

$$\langle j_g \rangle = 0.80 \text{ m/s}, \langle j_f \rangle = 0.21 \text{ m/s}.$$



(d) Churn turbulent flow

$$\langle j_g \rangle = 8.80 \text{ m/s}, \langle j_f \rangle = 0.20 \text{ m/s}.$$

Figure 4. Flow visualization in various flow regimes at $z/D_H=140$.

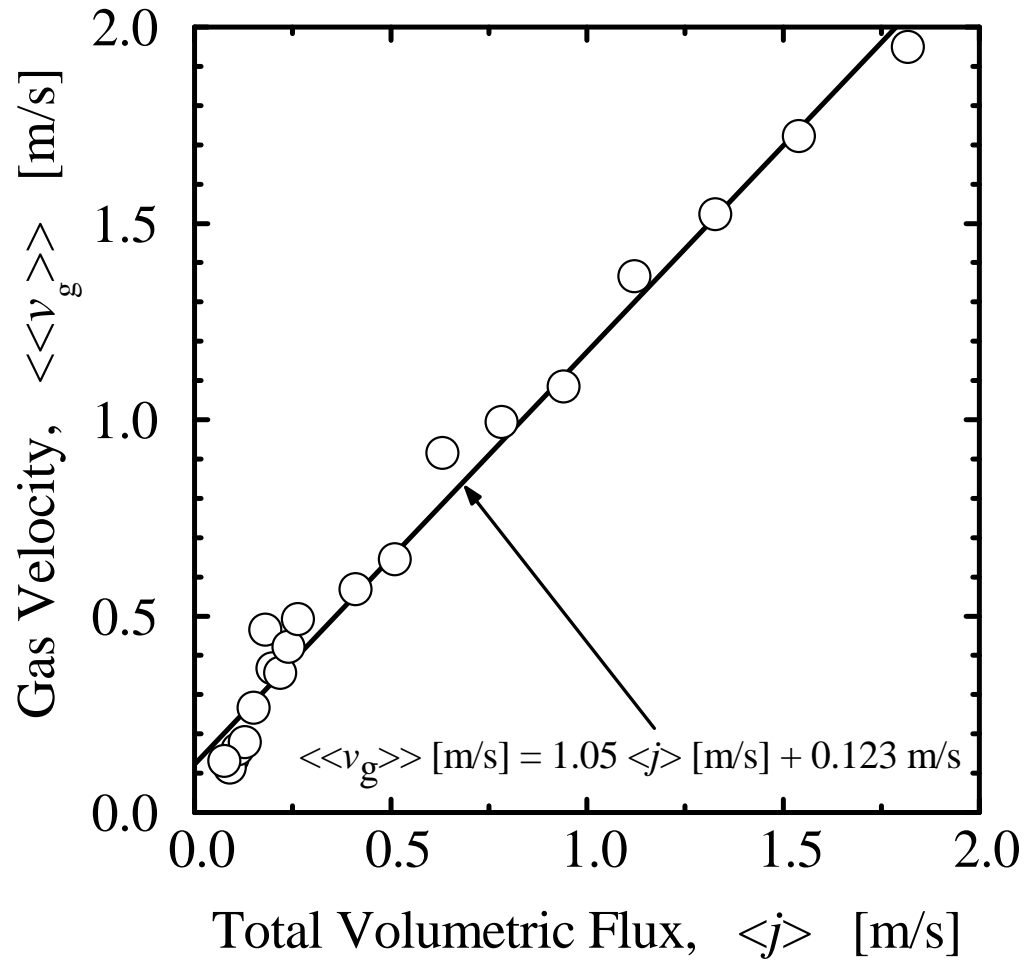


Figure 5. Drift-flux plot.

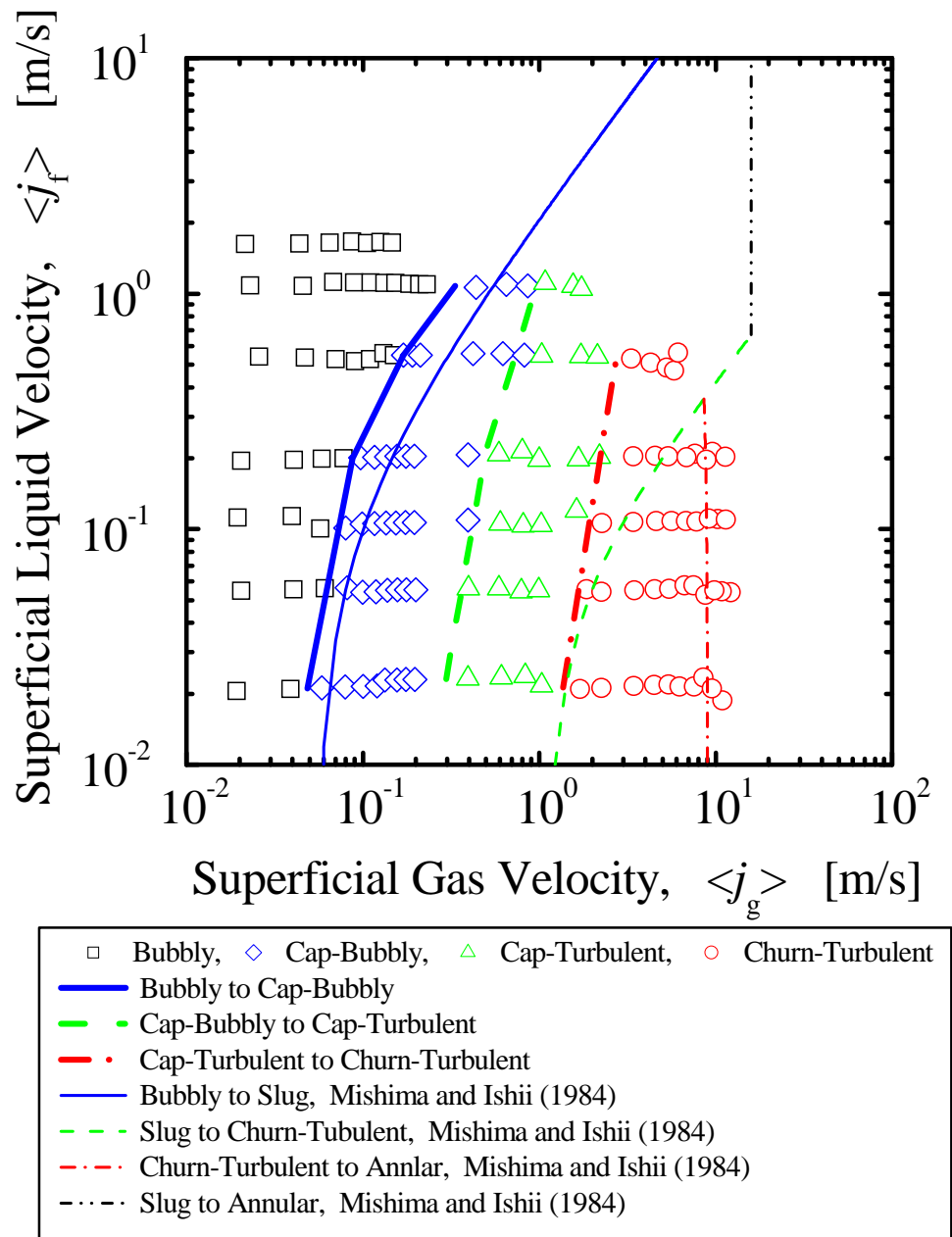


Figure 6. Experimental flow regime map at $z/D_H=200$.

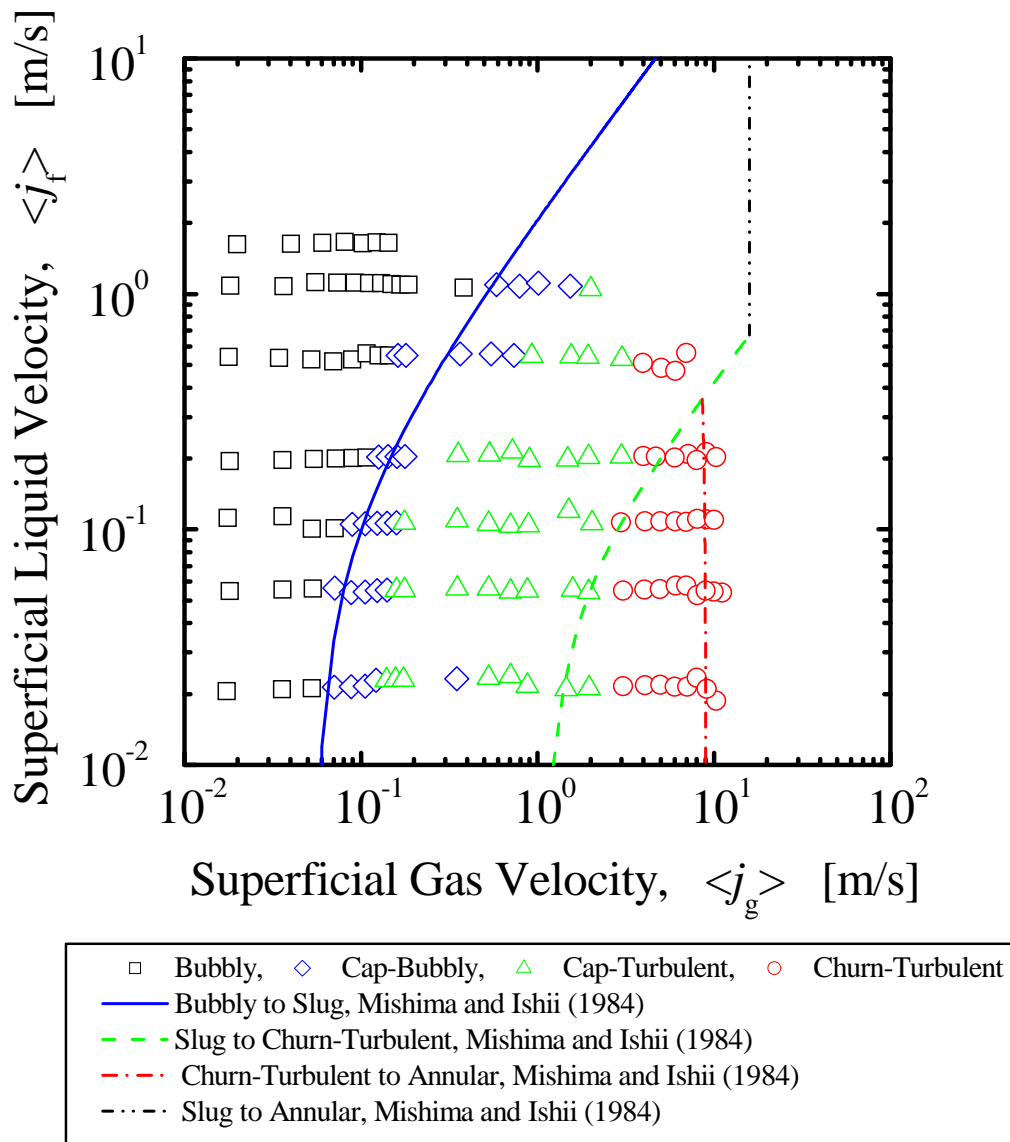


Figure 7. Experimental flow regime map at $z/D_H=7$.

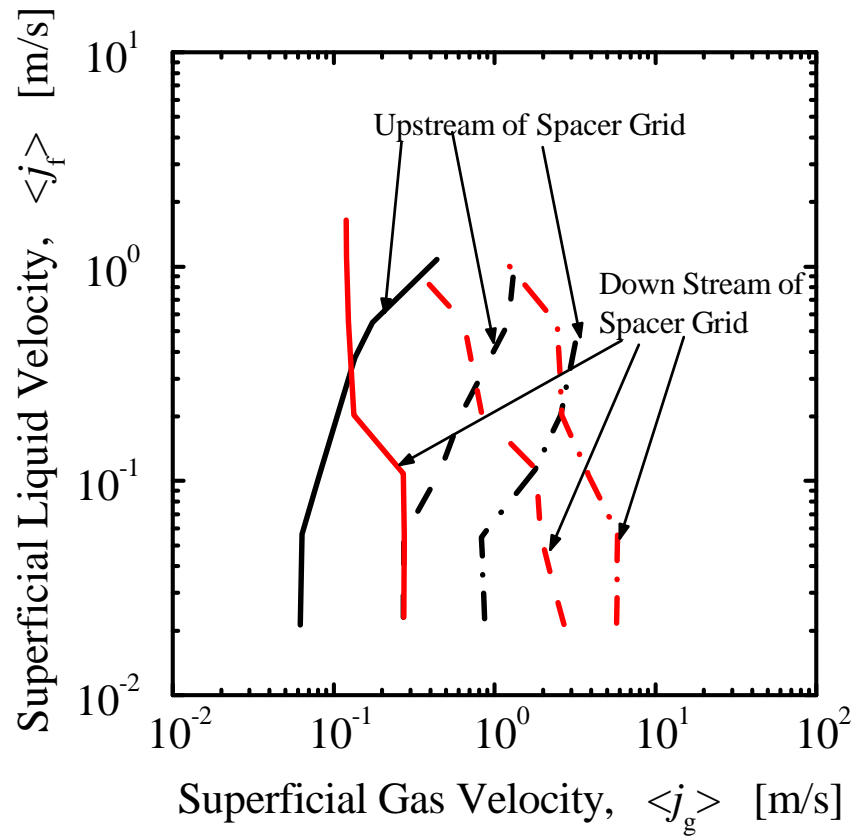


Figure 8. Experimental flow regime maps across the spacer grid at $z/D_H=121$, with upstream port at $z/D_H=116$ and downstream port at $z/D_H=124$.

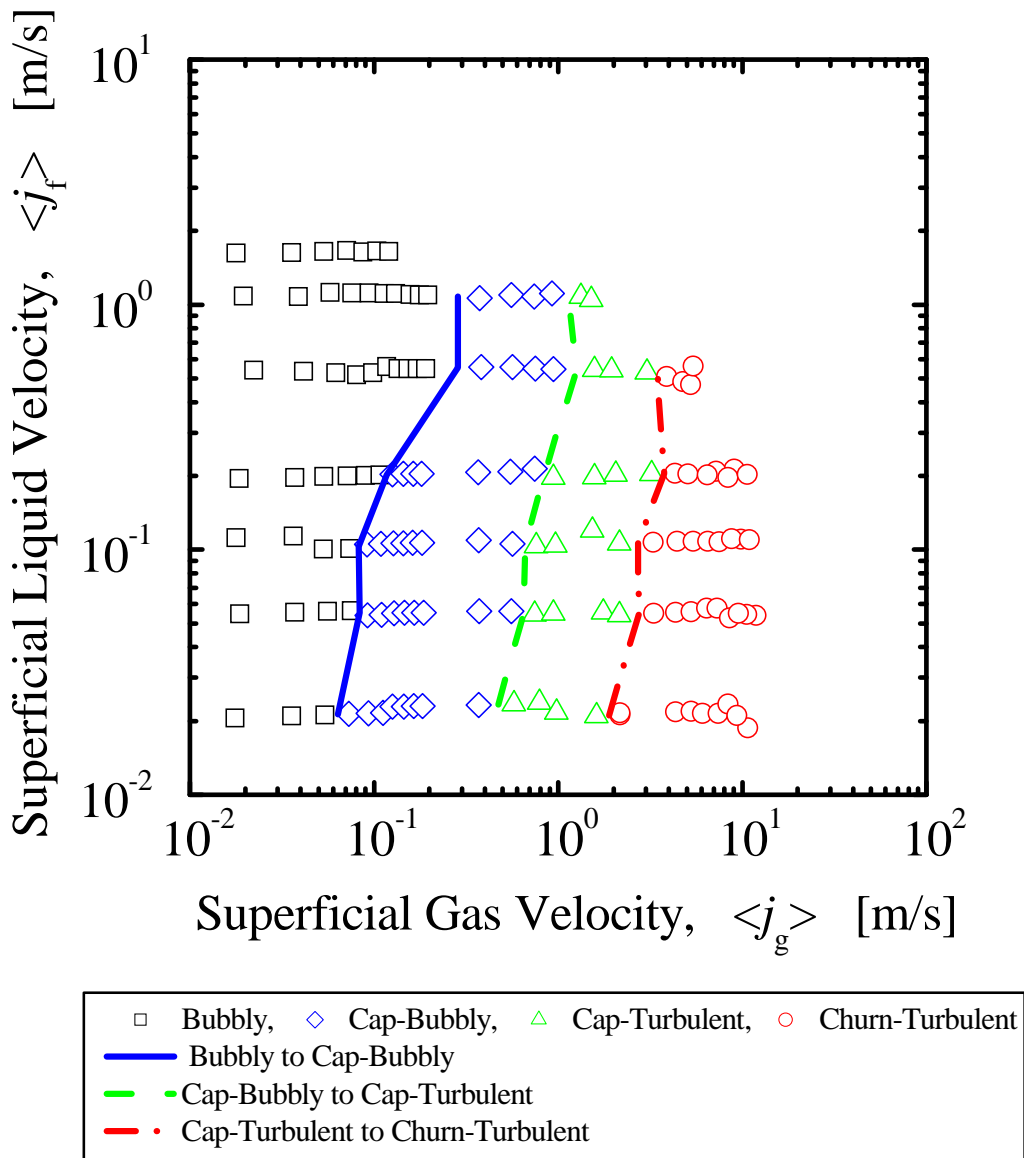


Figure 9. Experimental flow regime map at $z/D_H=137$.